Structural analysis of human MLKL bound with an activator SS-1-127

A thesis submitted by

Peiyun Sang

in partial fulfillment of the requirements for the degree of

Master of Science

In

Pharmacology and Drug Development

Tufts University

Graduate School of Biomedical Sciences

May 2024

Advisor: Alexei Degterev, Ph.D.

Abstract

As the executioner of Necroptosis, a programmed necrotic cell death, MLKL is a pseudokinase that can affect membrane integrity. The phosphorylation of MLKL by RIPK3 is essential for necroptosis as a cue for dimerization of pseudokinase domain of MLKL and further oligomerization. Here we report a compound SS-1-127 that binds to the pseudokinase domain of MLKL and will be investigated in the future for direct activation of this protein. We used protein purification and crystallography to obtain the structure of MLKL: SS-1-127 complex. The MLKL bound with SS-1-127 adopted a closed, active conformation, forming a head-to-tail, back-to-back dimer in crystal packing. SS-1-127 binds in the ATP-binding pocket of MLKL and forms various hydrogen bonds within the cleft, including the hydrogen bond with K230:E250 salt bridge conserved in active MLKL conformation. Compared with the structures of MLKL and P-MLKL, MLKL bound with SS-1-127 is in a new conformation. These observations suggest that binding of SS-1-127 helps maintaining the active conformation of MLKL and function as a substitution of phosphorylation to promote the dimerization of MLKL pseudokinase domain, thus inducing necroptosis.

In loving memory of my mentor, Dr. A. Andrew Bohm, whose guidance and wisdom light my path forward.

Acknowledgements

I extend my deepest gratitude to Dr. Alexei Degterev and Dr. Katya Heldwein, whose unwavering support and insightful guidance were pivotal in my journey through this project. Their mentorship not only shaped the course of my research but also enriched my personal and professional growth.

My heartfelt thanks go to all members of the Degterev and Heldwein Labs, with special acknowledgment to Gonzalo Gonzalez-Del Pino, Nathalie Lavoie, Bing Dai, Ariana Calderon-Zavala, and Yulia Dikusar. Your collective expertise, assistance, and camaraderie were indispensable, particularly in navigating the unique challenges we faced together.

I am profoundly thankful for Anamika Mourya, my colleague at Bohm Lab. Her companionship, wisdom, and support have been a source of strength and inspiration throughout this endeavor.

Lastly, I dedicate a special note of gratitude to my late mentor, Dr. A. Andrew Bohm. His influence extends beyond words, and his legacy continues to guide me. Dr. Bohm's teachings and values remain a beacon in my academic journey, and I am eternally grateful for the paths he helped me forge.

Table of Contents

Abstract ii

Dedication iii

Acknowledgements iv

Table of Contents v

List of Abbreviations vi

List of Tables vii

List of Figures viii

Chapter 1: Introduction 1
- 1.1. Overview of Necroptosis 1
- 1.2. Current structural studies of MLKL 1
- 1.3. Existing binders with MLKL 3
- 1.4. Oligomerization of MLKL 4

Chapter 2: Methods and Materials 6
- 2.1. Protein expression and purification 6
- 2.2. Crystallization and Optimization 7
- 2.3. Compound SS-1-127 9

Chapter 3: Results 10
- 3.1. Expression and purification of human MLKL 10
- 3.2. Crystallization and structure determination 10
- 3.3. Each protomer of the dimer is bound to SS-1-127 11
- 3.4. SS-1-127 binds in the ATP binding site of MLKL 16
- 3.5. Interfaces between two copies of MLKL in crystal cell units 16

Chapter 4: Discussion 19

Bibliography 21

List of Abbreviations

FADD - FAS-associated death domain protein
MLKL - Mixed lineage kinase domain-like protein
NFκB - Nuclear factor kappa-light-chain-enhancer of activated B cells
Ni-NTA - Nickel-Nickel-nitrilotriacetic acid
RIPK1 - Receptor-interacting serine/threonine-protein kinase 1
RIPK3 - Receptor-interacting serine/threonine-protein kinase 3
SDS-PAGE - sodium dodecyl sulfate-polyacrylamide gel electrophoresis

List of Tables

Table 2.1 Data collection and refinement statistics for MLKL: SS-1-127 complex structure.....8

List of Figures

Figure 1.1 Mouse MLKL-RIPK3 complex. 2
Figure 1.2 MLKL construct, mouse full-length MLKL structure and two conformations of MLKL. 4
Figure 1.3 Chemical structures of existing binders of MLKL 4
Figure 2.1 Chemical structure of SS-1-127. 9
Figure 3.1 Domain structure of MLKL and protein construct purified. 10
Figure 3.2 Crystals of human MLKL: SS-1-127 complex from sitting drop crystallization screens. 11
Figure 3.3 The overall structure and superimpose of two copies of human MLKL: ss-1-127 complex. 12
Figure 3.4 Illustration of features of MLKL in an active conformation 14
Figure 3.5 Side by side comparison with structured MLKL models and superimposing comparison with models with partly structured activation loops. 15
Figure 3.6 SS-1-127 binds in the ATP binding pocket of MLKL. 17
Figure 3.7 Interface interactions between two copies of MLKL. 18
Figure 4.1 Superimposing comparison of MLKL, P-MLKL, Chain A, Chain B and MLKL bound with Cpd 4 20

Chapter 1: Introduction

1.1. Overview of Necroptosis

Necroptosis, also known as programmed necrosis, is a mechanism of caspase-independent, regulated cell death[1-3]. Necroptosis is dysregulated in various human diseases, such as inflammatory diseases, ischemia-reperfusion injury and inflammatory bowel disease[4-8]. Necroptosis can detect pathogens and promote tissue repair, which occurs after the tumor necrosis receptor (TNFR1) is activated by TNFα[9]. The activation of TNFR1 is not the only one that can trigger necroptosis. The activation of other cellular receptors can also trigger necroptosis, including death receptors, Toll-like receptors (TLR3,TLR4) and cytosolic nucleic acid sensors[10-13]. Most of the these mentioned pathways trigger NF-κB-dependent signals. When there is no activity of caspase-8, RIPK1 recruits and phosphorylates RIPK3, thus forming a necrosome complex[1, 14]. The RIPK1/RIPK3 necrosome complex can recruit and phosphorylate MLKL [15, 16]. After the phosphorylation of MLKL, a conformational change is induced, causing the exposure of the N-terminal 4-helix bundle domain of MLKL, turning MLKL into the executor of necroptosis. Two models are hypothesized to explain how MLKL inflicts cell lysis. It is clear that MLKL oligomer inserts into the plasma memebrane. Some data suggest that it may function as an ion pore, which leads to cell swelling and cell rupture[17, 18]. Another hypothesis is that MLKL pore directly disrupts membrane integrity, leading to cell lysis[19, 20].

1.2. Current structural studies of MLKL

MLKL consists of an N-terminal coiled-coil domain and a C-terminal pseudokinase domain. The C-terminal pseudokinase is responsible for association with RIPK3[21]. MLKL is highly conserved, with 69%/81% sequence

identity/similarity for the pseudokinase domains of human and mouse MLKL. In 2013, Xie et al first presented the crystal structures of pseudokinase domain of mouse MLKL and mouse RIPK3: MLKL complex[22]. For the pseudokinase domain of mouse MLKL, the N-lobe contains an antiparallel, five-stranded β-sheet ad an α-helix while the C-lobe comprises seven α-helices and a pair of β-strands, displaying a kinase fold that is indistinguishable to other protein kinases (as show in blue in Figure 1.1). Structurally. MLKL is classified as a pseudokinase due to the fact that in its HRD motif of the catalytic loop and DFG motif there is absence of ASP. In the structure of inactive open confirmation of MLKL, unlike in active protein kinases, in which there is a conserved Lysine within ATP-binding VAIL sequence, the canonical αC helix position of inactive MLKL is occupied by a short helix formed by the N-terminal segment of activation loop (as shown in pink in Figure 1.1)[23, 24].

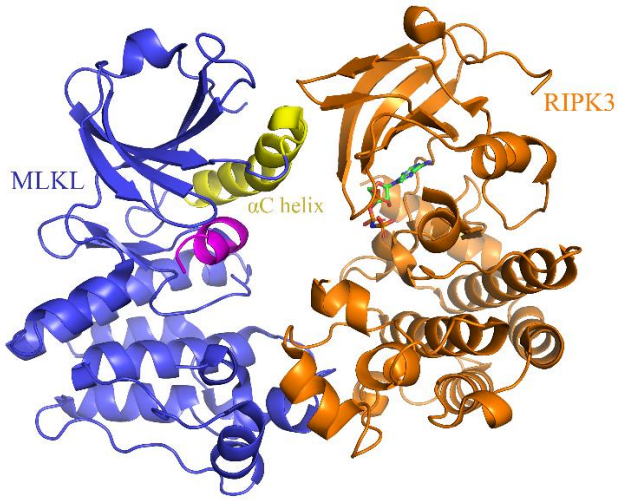

Figure 1.1 mouse MLKL-RIPK3 complex.
RIPK3(orange); MLKL (blue); For MLKL, the αC helix is shown in yellow and activation loop helix is shown in pink (PDB code: 4M69). All figures of structures were drawn using PyMOL. (http://www.pymol.org/)

In 2013, Murphy et al first presented the crystal structure of full-length mouse MLKL[16]. From the structure of full-length mouse MLKL, they revealed that the N-

terminal domain consists of a four-helix bundle followed by a two-helix brace, which connects the four-helix bundle to the pseudokinase domain (Figure 1.2(B)). MLKL pseudokinase domain were found to present two different conformational states[25]. As described before in mouse MLKL structure, in inactive MLKL, a short helix is formed in activation loop, occupiing the position of αC helix in active MLKL (Figure 1.2(C)). In active closed MLKL model, the side chains of Ile265, Met254, Phe350 and His329 are forming a hydrophobic regulatory R-spine which is conserved in closed active kinases[25, 26]. Also, there is a salt bridge observed between Lys230 of VAIK motif and Glu250 from αC helix. In vivo, the conformational change of MLKL happens during disengagement from RIPK3[27].

1.3. Existing binders with MLKL

Based on PDB search, there are three compound binders that bind to MLKL pseudokinase domain found and have been structured (Figure 1.3). Cpd 1 and Cpd 4 are ATP-competitive binders[28]. Cpd 1 is a type II kinase inhibitor, which is reported to bind to other kinases, and can block necroptosis[29]. Cpd 4 is a type I inhibitor. Cpd 1 binds in the ATP binding site of MLKL by making two hydrogen bonds with the backbone amide and carbonyl of the hinge. Cpd 4 also binds in the ATP binding site of MLKL, making two hydrogen bonds with the hinge and have hydrogen bonds with two nearby water molecules[28].

Another molecule, Compound 2 is a type II binder that can bind to all three necroptotic effector proteins (MLKL, RIPK1 and RIPK3)[30]. It binds in the ATP binding pocket of MLKL and forms three hydrogen bonds with Glu250, Cys286 and Gly349.

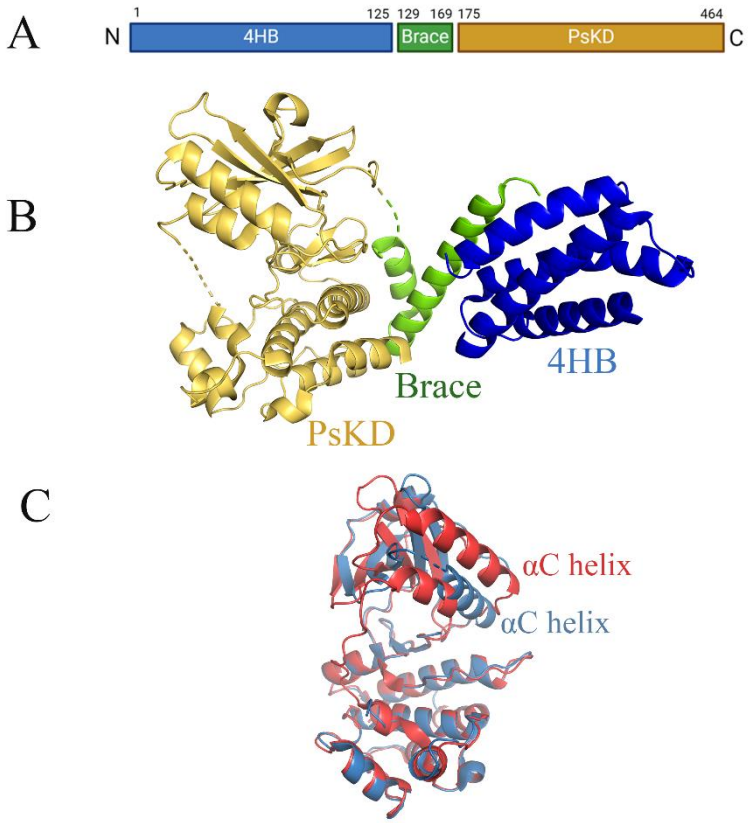

Figure 1.2 MLKL construct, mouse full-length MLKL structure and two conformations of MLKL.
A: MLKL comprises three parts. B: crystal structure of full-length mouse MLKL (PDB code: 4BTF). C: Superposition of active and inactive human MLKL. Active MLKL is shown in blue (PDB code: 7JW7), Inactive MLKL is shown in red (PDB code: 7JXU)

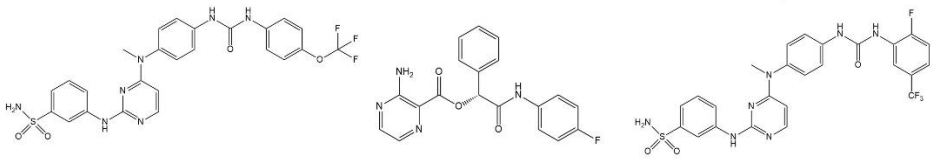

Cpd 1 Cpd 4 Compound 2

Figure 1.3 Chemical structures of existing binders of MLKL

1.4. Oligomerization of MLKL

Phosphorylation of the MLKL pseudokinase domain by the RIPK3 kinase can lead to MLKL oligomerization, prior to plasma membrane translocation[29, 31, 32]. The phosphorylation sites of MLKL by RIPK3 are mainly threonine 357 and serine

358 of human MLKL (serine 345 for mouse MLKL), which are part of the activation loop[21]. The activation loop phosphorylation can promote MLKL oligomerization through the coiled-coil domain mediated self-assembly[17, 33]. Additional modifications on the MLKL were found to promote oligomerization. It is reported that the phosphorylation by RIPK3 of MLKL can induce the dimerization of the pseudokinase domain of MLKL[34, 35]. The dimerized MLKL pseudokinase domain can subsequently promote the formation of homotetramers of MLKL. The tetramer formation of MLKL is an essential step, enabling 4-helix bundle domains of MLKL to release, thus causing permeabilization and cell death[35]

Chapter 2: Methods and Materials

2.1. Protein expression and purification

Pseudokinase domain of human MLKL was constructed by sub-cloning residue 191- 471 of the pseudokinase domain of human MLKL cDNA, with the dual mutations of E366A and K367A, into a pET15b vector with a thrombin cleavable N-terminal six histidine fusion tag. BL21(DE3) *Escherichia coli* cells were transformed with the plasmids encoding either pseudokinase protein construct and were grown at 37℃ in LB media supplemented with ampicillin to an OD of 0.6. The temperature was reduced to 18℃ and protein expression was induced by adding 0.1mM IPTG and shaking for an additional 16 hours. The cells were harvested and resuspended in lysis buffer (50mM Tris pH 8.0, 250mM NaCl, 1mM $MgCl_2$, 10% Glycerol, 0.1mM PMSF, 0.25% IGEPAL and Pierce™ EDTA-free protease inhibitor tablet, Thermo Fisher) and were lysed using high-pressure homogenizer (EmulsiFlex-C5, AVESTIN, Inc, Canada). The lysate was clarified by ultracentrifugation at 10,000 x g for 30 minutes at 4℃ and the supernatant was loaded onto Ni-NTA column equilibrated with lysis buffer. The Ni-NTA agarose beads were washed with lysis buffer supplemented with 50mM imidazole pH 8.0 and 0.02% 2-Mercaptoethanol. Then the protein was eluted with lysis buffer supplemented with 120mM imidazole pH 8.0 and 0.02% 2-Mercaptoethanol. After analysis using SDS-PAGE gel, the fractions were pooled and concentrated using MilliporeSigma™ Amicon™ Ultra-15 centrifugal filter. The concentration of NaCl was diluted to 70mM and thrombin was added 1:1000 (weight: weight) for overnight His-tag cleavage digestion at room temperature. The His-tag liberated protein was further purified using SOURCE™ Q anion exchange column (Sigma-Aldrich) with buffer A (25mM MES pH 6.0, 20% glycerol, 0.1% 2-

Mercaptoethanol) and buffer B (25mM MES pH 6.0, 20% glycerol, 0.1% 2-Mercaptoethanol, 1M NaCl). The protein was eluted during gradient elution from 7% buffer B to 40% buffer B at 2ml/min for 1 hour. After SDS-PAGE gel analysis, the fractions were pooled and exchanged into storage buffer (20mM Tris pH 8.0, 20% glycerol, 2mM DTT, 200mM NaCl). The batch giving proteins were concentrated to 1.15mg/ml and snaped frozen in dry ice and ethanol, kept in -80℃ fridge before setting up crystal screening.

2.2. Crystallization and Optimization

For crystallization, aliquots of human MLKL pseudokinase domain was incubated with ss-1-127 for 1 hour over ice. 1.15 mg/ml protein and ten-fold molar excess of ss-1-127 were used. NeXtal Classics and Pegs Suite screens were used as the initial screens for crystallization using the sitting drop vapor diffusion method at room temperature. The crystallization drops consisted 0.1µl of the reservoir solution and 0.1µl of the protein solution during initial screening. Plate-shaped crystals suitable for structure determination were obtained by vapor diffusion in hanging drops using a reservoir solution: 0.1M MES pH 6.5, 20% (w/v) PEG 4K, at room temperature with three drops in a well. Crystals were harvested and flash frozen in liquid nitrogen. X-ray diffraction data was collected at a wavelength of 1.1159 Å at Beamline 8.3.1 of the Advanced Light Source, Berkley. Data were integrated and merged using Xia2 suite. The initial structure was phased by PHENIX.PHASER-MR using PDB entry 5KNJ as an initial search model. Compound ss-1-127 was placed into positive density in an initial F_o-F_c map and included in subsequent rounds of refinement using PHENIX.REFINE. Successive manual refinement was performed using COOT. The data collection and refinement statistics are presented in Table 2.1. All Figures of

structures were drawn using PyMOL (http://www.pymol.org/).

Table 2.1 Data collection and refinement statistics for MLKL: SS-1-127 complex structure

	MLKL bound with SS-1-127
Wavelength	1.116
Resolution range	63.79 - 2.9 (3.004 - 2.9)
Space group	P 1 21 1
Unit cell	48.72 127.59 55.65 90 116.15 90
Total reflections	92457 (9077)
Unique reflections	13412 (1331)
Multiplicity	6.9 (6.9)
Completeness (%)	99.77 (99.40)
Mean I/sigma(I)	5.58 (0.90)
Wilson B-factor	56.45
R-merge	0.6521 (2.178)
R-meas	0.7052 (2.355)
R-pim	0.2663 (0.8884)
CC1/2	0.608 (0.331)
CC*	0.87 (0.705)
Reflections used in refinement	13521 (1323)
Reflections used for R-free	547 (55)
R-work	0.2241 (0.3583)
R-free	0.2671 (0.4220)
CC(work)	0.246 (0.091)
CC(free)	0.184 (0.106)
Number of non-hydrogen atoms	4246
macromolecules	4159
ligands	128
solvent	15
Protein residues	519
RMS(bonds)	0.003
RMS(angles)	0.51
Ramachandran favored (%)	95.03
Ramachandran allowed (%)	4.97
Ramachandran outliers (%)	0
Rotamer outliers (%)	1.31
Clashscore	15.14
Average B-factor	62.37
macromolecules	62.24
ligands	74.04

2.3. Compound SS-1-127

SS-1-127 is provided by Degterev Lab, Tufts University. The synthesis routine is unpublished, thus not included.

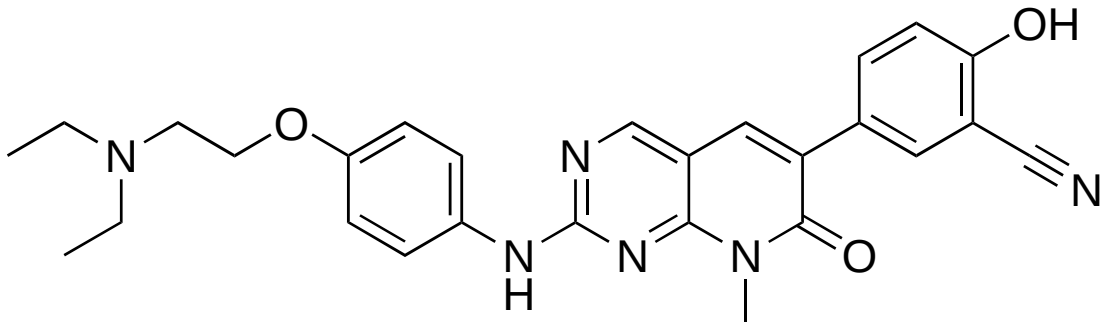

Figure 2.1 Chemical structure of SS-1-127.

Chapter 3: Results

3.1. Expression and purification of human MLKL

For crystallization of MLKL: SS-1-127 complex, we used the pseudokinase domain of human MLKL (residues 191 - 471) with the E366A and K367A mutations. The dual mutations were identified as having high surface entropy and were mutated to alanine to improve crystal packing[28]. After the initial Ni-NTA purification and thrombin His-tag cleavage, a further SOURCE™ Q anion exchange column was used (Figure 3.1).

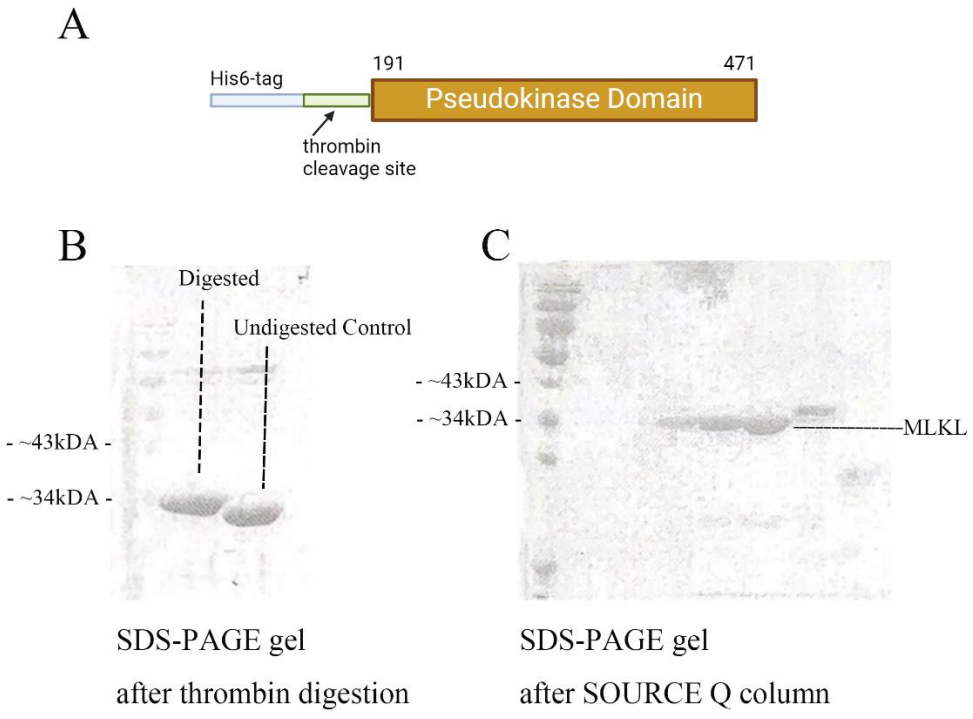

Figure 3.1 Domain structure of MLKL and protein construct purified.
A: Construct of MLKL. B: SDS-PAGE gel after thrombin digestion to cleave the His6-tag. C: SDS-PAGE gel after SOURCE Q column

3.2. Crystallization and structure determination

Crystals of the human MLKL: SS-1-127 complex initially appeared in one condition: 0.1M MES pH 6.5, 25% (w/v) PEG 4K. The condition was repeated and

optimized in 6μL hanging drop format in 24-well plates. The crystals were plates, belonging to the space group $P12_11$ (Figure 3.2). The final structure was solved to 2.9Å, with R_{work}/R_{free} of 0.22/0.27. Data were integrated and merged using Xia2 suite. The initial structure was phased by PHENIX.PHASER-MR using PDB entry 5KNJ as an initial search model. Compound ss-1-127 was placed into positive density in an initial F_o-F_c map and included in subsequent rounds of refinement using PHENIX.REFINE. Successive manual refinement was performed using COOT.

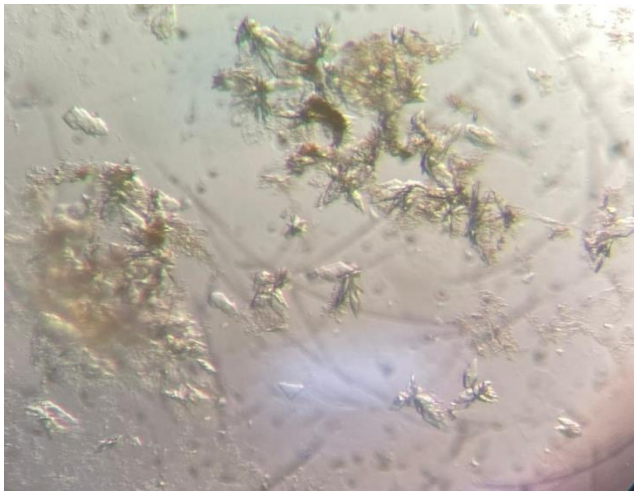

Figure 3.2 Crystals of human MLKL: SS-1-127 complex from sitting drop crystallization screens.
Further rounds of optimization yielded larger.

3.3. Each protomer of the dimer is bound to SS-1-127

For MLKL: SS-1-127 complex structure, after refinement, residue 191-470 of human MLKL pseudokinase domain are modeled in the crystal structure. Compared with the construct, residue189-190, residue 235-238 and residue471 could not be modeled due to a lack of electron density. There are two copies found in crystal asymmetrical cell unit, chains A and B, forming a head-to-tail, back-to-back dimer (Fig 3.3(A)). For each copy, the N-lobe comprises an antiparallel, five stranded β-sheet, and an activation of αC helix. The C-lobe contains seven α-helices and an

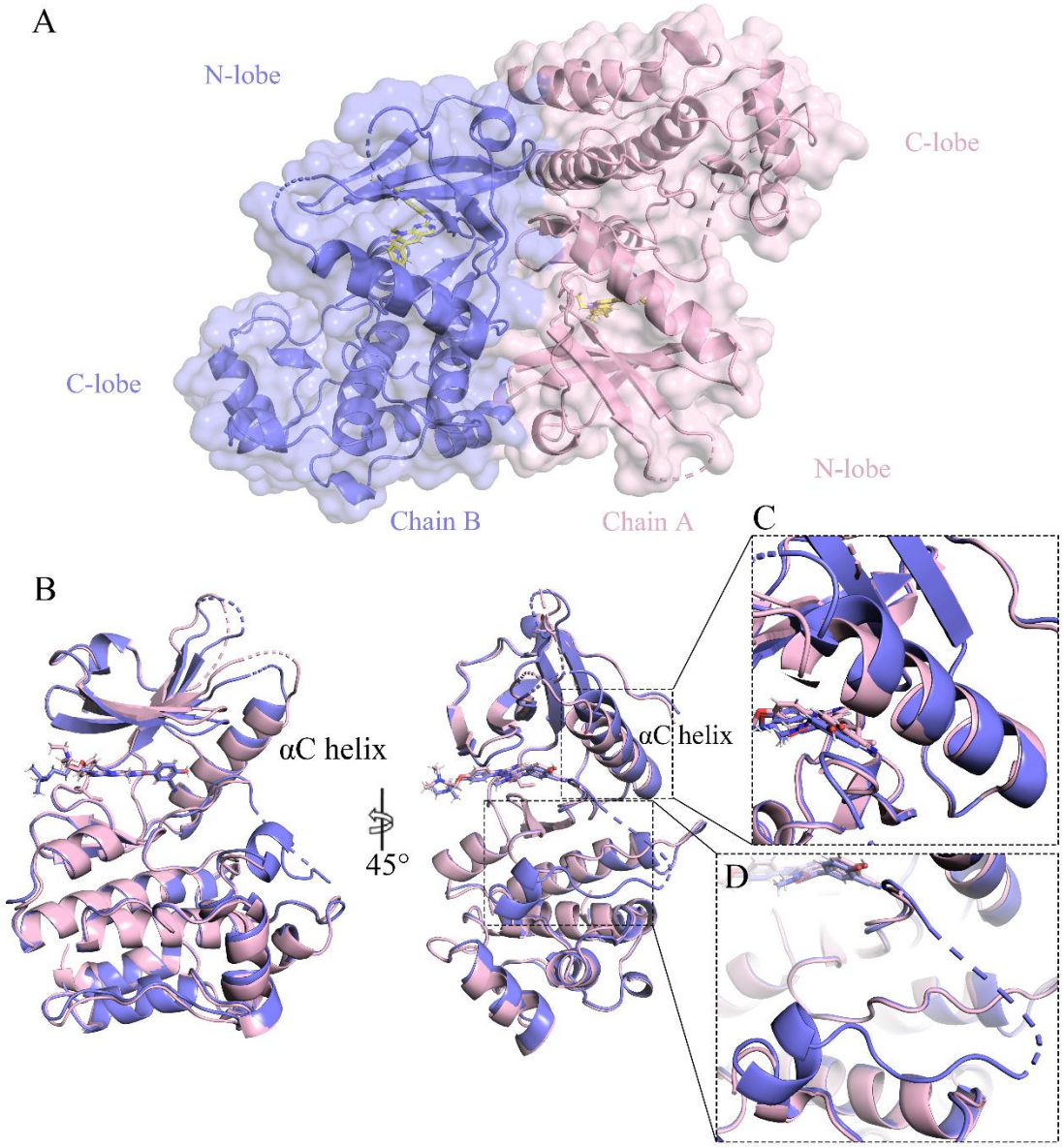

Figure 3.3 The overall structure and superimpose of two copies of human MLKL: ss-1-127 complex.
Chain A is shown in Pink and Chain B is shown in purple. A: overall view of structured MLKL pseudokinase domain; B: Superimposing comparison of Chain A and Chain B; C: Enlarged view of the superimposed αC helix part; D: Enlarged view of superimposed activation loops of Chain A and Chain B.

antiparallel, two stranded β-sheet. Two copies of pseudokinase domain observed in crystal structure (pink for chain A and purple for chain B) are superimposed in Figure 3.3(B). Most elements superpose well, but several β-strands of N-lobe vary in length

(RMSD: 0.431). The αC helix in two chains are positioned at a slightly different angles in relation to N-lobe (Figure 3.3(C)). In chain B, residues 367-371 are forming a helix, while the same sites of chain A could not be modeled due to a lack of electron density.

Both chains of our structure are adopting an active conformation. As shown in Figure 3.3(B), there is no helix of activation loop formation near the αC helix. As shown in Figure 3.4(C, D), the side chains of Ile265, Met254, Phe350 and His239 (shown as yellow stick from top to bottom) form a hydrophobic regulatory 'R'-spine synonymous on both copies. As shown in Figure 3.4(A, B), the conserved salt bridge between K230 and E250 was observed. Together, these results indicates that in MLKL: ss-1-127 complex, our human MLKL adopted a closed, active formation.

Compared with other published structures of human MLKL pseudokinase domain, the activation loop in chain A of our structure is adopting a new conformation (Figure 3.5). The 4MWI, 6LK5, 6LK6 structures contain the MLKL pseudokinase domain alone, with different mutations. The short helix of activation loop formed in Chain B near the C-lobe is different from other structures, which implies that binding of SS-1-127 induces a conformational change (Figure 3.5(B)). The formation of the short helix also may result from crystal cell packing. The activation loop was not modeled in Chain A due to a lack of density, which is suggesting that the activation loop is still dynamic. The N-lobe of Chain A and Chain B have shifts compared to MLKL alone (Figure 3.5(C)). The αC helix shifted deviated and both chains shifted in the same direction, with an angle from MLKL alone structure.

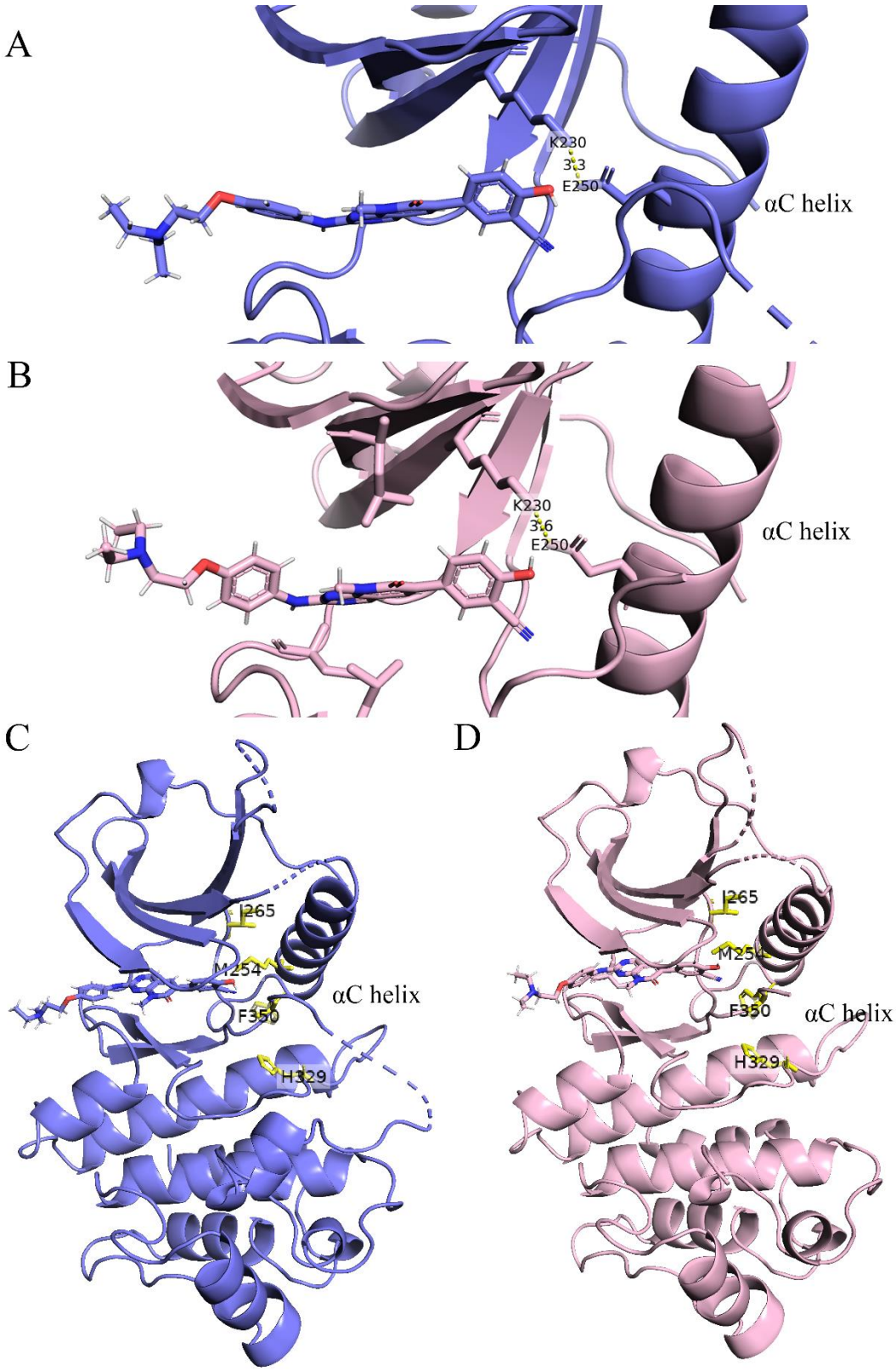

Figure 3.4 Illustration of features of MLKL in an active conformation
β3 strand lysine: αC helix glutamate (K230:E250) salt bridge (A, B) and aligned R-spine of MLKL: SS-1-127 complex (C, D). Chain A is shown in Pink and Chain B is shown in purple.

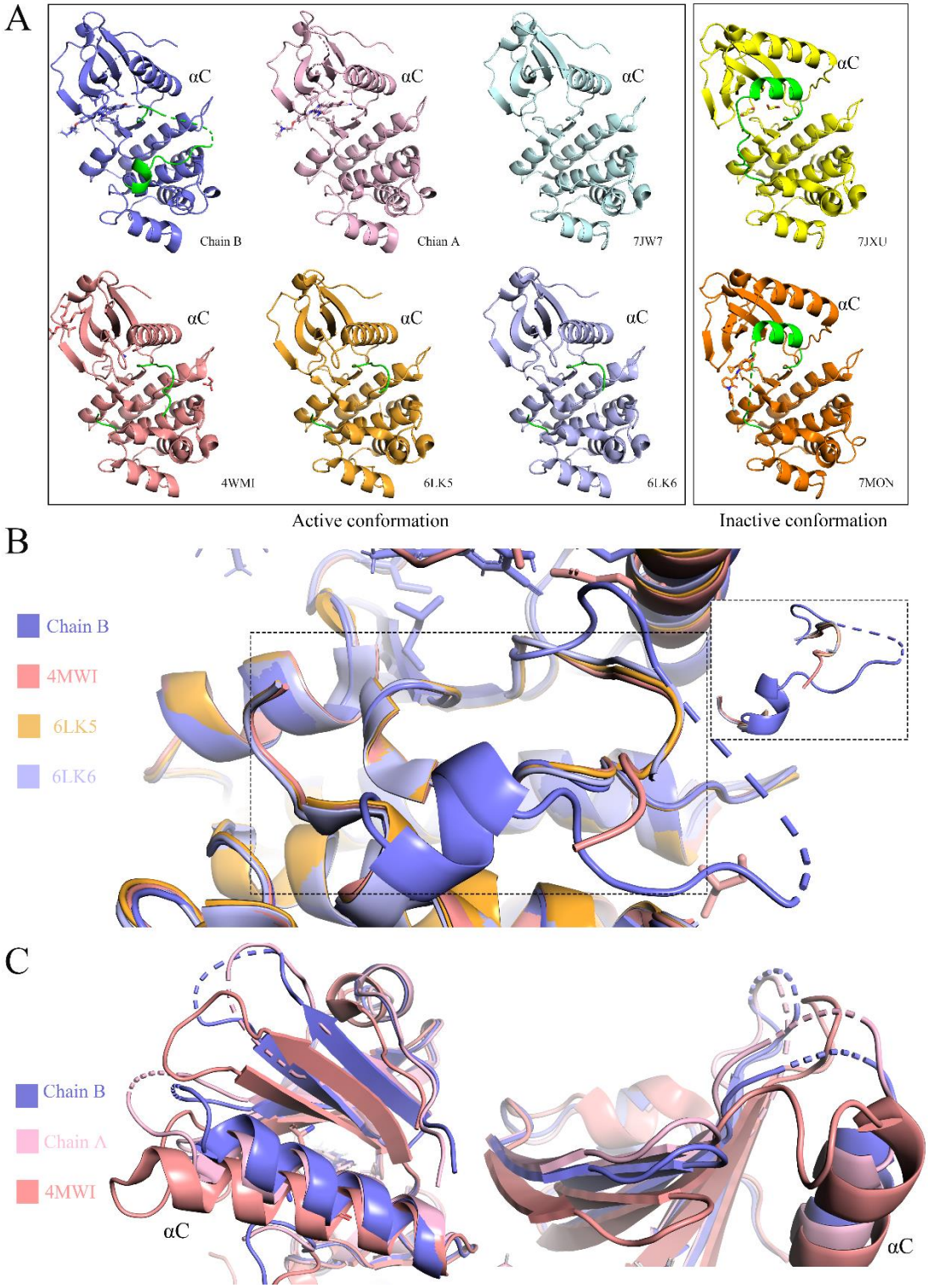

Figure 3.5 side by side comparison with structured MLKL models and superimposing comparison with models with partly structured activation loops.
A: Side by Side comparisons of MLKL structures. The activation loops are shown in green; B: Superimposing comparison of MLKL structures in active conformation with activation loops modeled. The enlarged truncated view is shown on the right; C: Superimposing comparison of Chain A, Chain B and active MLKL alone (4WMI).

3.4. SS-1-127 binds in the ATP binding site of MLKL

SS-1-127 is binding to the ATP binding site of MLKL and forming hydrogen bonds with residues. As shown in Figure 3.6 (A, B), The 2-hydroxyl group of Benzonitrile on SS-1-127 is forming hydrogen bonds with Lys230 and Glu250, which are forming the conserved salt bridge in active MLKL. Also, the Cys286 is forming a hydrogen bond with the 2-amide of backbone from compound. The side chains of Leu217 and Leu338 on both copies are adopting a position that are towards the heterocyclic part of ss-1-127, functioning as a clamp to help stabilize the compound. The salt bridge between β3 strand lys230 and αC helix Glu250 is a feature found in MLKL in active conformation, suggesting that SS-1-127 is helping maintaining the closed, active conformation.

Due to the lack of stable density on both copies, the [(N, N-diethylamino) ethyl] alkoxyl tail of the compound is not in a fixed position and should be flexible, with no interactions with MLKL.

3.5. Interfaces between two copies of MLKL in crystal cell units

Among the interface between two copies of MLKL in crystal cell units, hydrogen bonds and salt bridges are formed (Figure 3.7(A)). Overall, the hydrogen bonds and salt bridges formed among interface are mostly symmetrical. For both copies, the side chain of Arg224 forms two salt bridges with the side chain of Asp460 in the other copy (Figure 3.7(B, E)). Along with Asp460: Arg224 salt bridge, symmetrical interactions including hydrogen bonds between Tyr222: Arg319, Lys194: Lys255 and Ser259: Arg264 as well as salt bridges between Lys194: Glu258, Glu258: Arg 264. The only asymmetrical hydrogen bond formed is between Lys256 and Lys194.

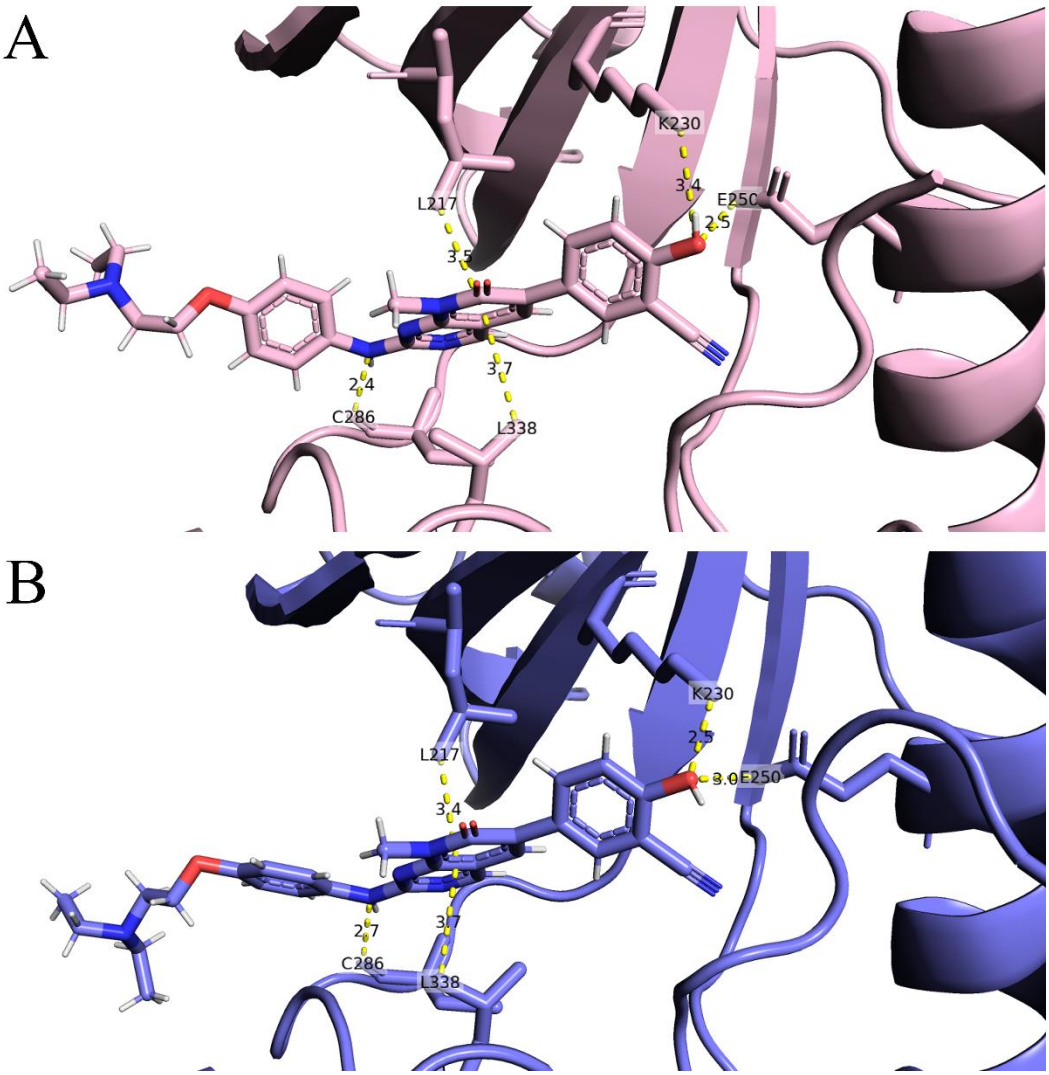

Figure 3.6 SS-1-127 binds in the ATP binding pocket of MLKL.
Chain A is shown in pink and Chain B is shown in purple.

Based on the PDBePISA calculation, around 38-40 residues are involved among the interface. The interface scored 0.00 in Complex Formation Significance Score (CSS), which is a tool to estimate the interface relevance to complex formation increases. Current score implies that this interface may not play any role in complex formation and may be just a result of crystal packing only. However, while our crystal packed in P1 21 1, there are phosphorylated MLKL dimers reported, whose crystals have a different space group, C2 2 21[34, 35]. Since very similar dimers are observed in different crystal space groups, this suggests that this dimer is biologically relevant.

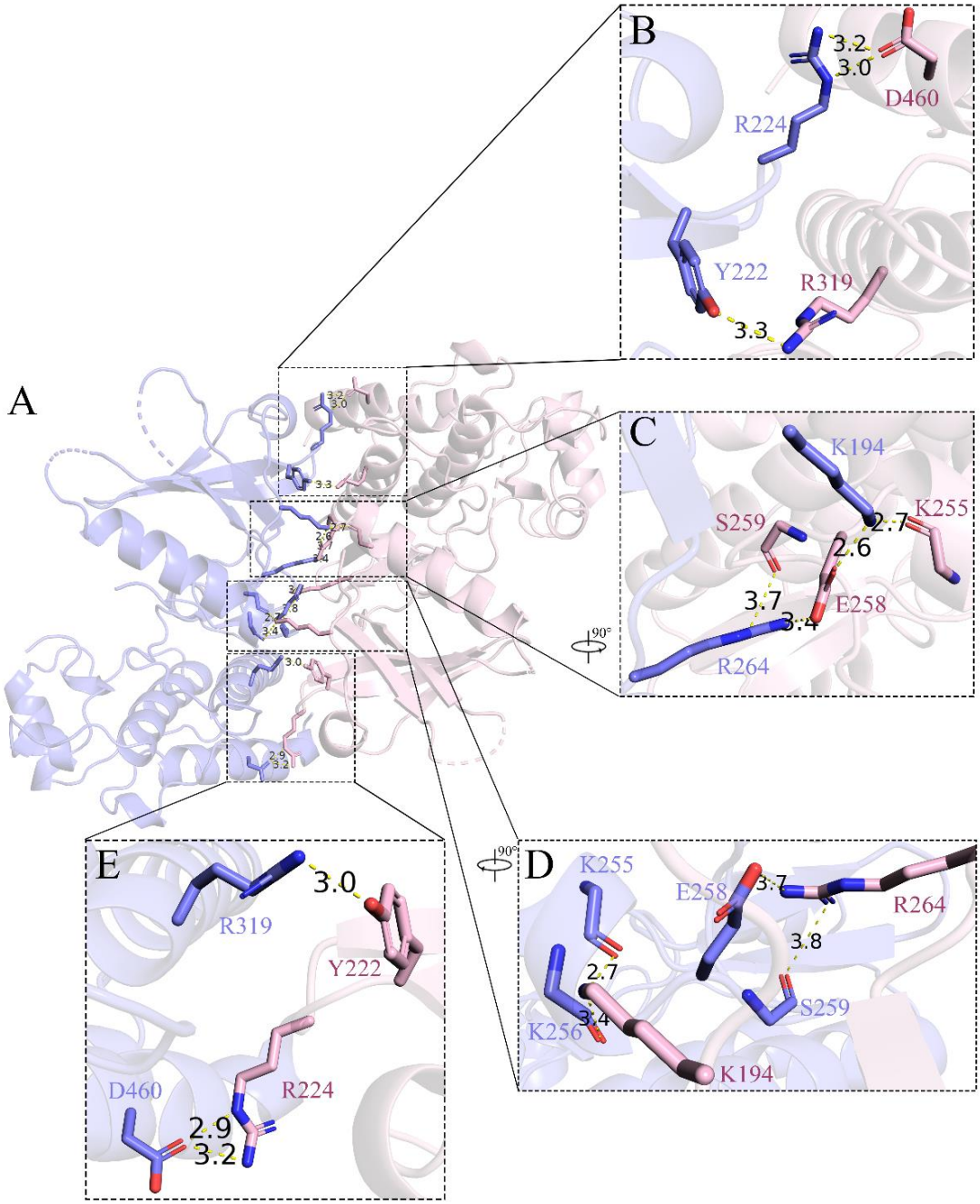

Figure 3.7 Interface interactions between two copies of MLKL.
The interface residues are shown in sticks. A: overview of the interface between two copies. B, C, D, E: enlarged view of the interface interactions.

Along with the experiment results that SS-1-127 induces necroptosis even without the presence of RIPK3 (Degterev Lab, unpublished data), this may imply that binding of SS-1-127 may promote dimerization of MLKL pseudokinase domain, which is an essential and critical step in necroptosis.

Chapter 4: Discussion

MLKL is executioner of necroptosis and the exact mechanism of MLKL's affecting the membrane integrity still remains unclear. Here, we found the compound SS-1-127 as a binder and presented the human MLKL: SS-1-127 complex structure. After MLKL binding with SS-1-127, it adopts a different closed, active conformation and packed a s a dimer in crystal cell units. Experiment results show that SS-1-27 can induce necroptosis with the absence of RIPK3 (Degterev Lab, unpublished data).

Cpd4 binds roughly the same conformation of MLKL as SS-1-127 but lacks activity to affect necroptosis. When comparing with MLKL, phosphorylated MLKL have slight shifts of β-sheet and loop formed by D271-Q278 (Figure 4.1(A)). Although Cpd 4 has no activity on MLKL, structure of MLKL bound with Cpd4 also have similar shifts of β-sheet and loop formed by D271-Q278 in the same direction (Figure 4.1(B)). This may imply that there is another transitional state between, which is critical for the dimerization of MLKL.

While there are only phosphorylated MLKL dimers structures reported, our structure is the first one with the dimerization of unphosphorylated MLKL[35]. For MLKL bound with SS-1-127, both Chain A and Chain B present significant shifts on the N-lobe, including the angular deviation of αC helix, the position shifts of β-sheet and loop formed by D271-Q278 (Figure 4.1(C)). Along with the results that SS-1-127 can induce necroptosis without RIPK3 (Degterev Lab, unpublished data), this implies that after binding with SS-1-127, MLKL is undergoing a new conformational change that is similar to the conformational change after being phosphorylated. Based on the observed interactions, we hypothesis that the hydrogen bonds between Lys230, Glu250 and the 2-hydroxyl group of Benzonitrile on SS-1-127 may be critical to

induce the conformational change. The [(N, N-diethylamino) ethyl] alkoxyl tail of SS-1-127 is dynamic, taking the space near the cleft, which may help to keep the brace domain out to help form the coiled coil, which is proposed to drive the tetramerization.

Our compound can be useful to look deeper into the oligomerization process of MLKL. Also, SS-1-127 can be a starting point to design better necroptosis activator based on the atomic interactions found.

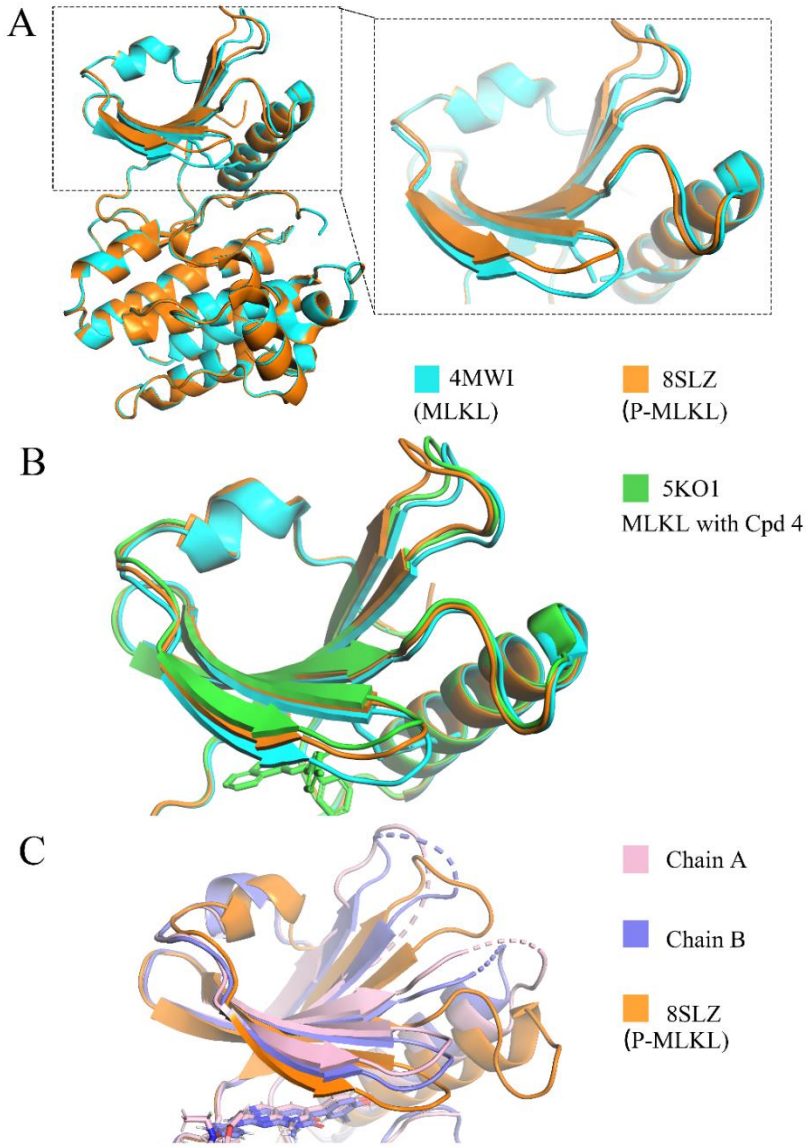

Figure 4.1 Superimposing comparison of MLKL, P-MLKL, Chain A, Chain B and MLKL bound with Cpd 4.

Bibliography

[1] Y.S. Cho, S. Challa, D. Moquin, R. Genga, T.D. Ray, M. Guildford, F.K. Chan, Phosphorylation-driven assembly of the RIP1-RIP3 complex regulates programmed necrosis and virus-induced inflammation, Cell 137(6) (2009) 1112-23.

[2] D. Bertheloot, E. Latz, B.S. Franklin, Necroptosis, pyroptosis and apoptosis: an intricate game of cell death, Cell Mol Immunol 18(5) (2021) 1106-1121.

[3] A. Degterev, Z. Huang, M. Boyce, Y. Li, P. Jagtap, N. Mizushima, G.D. Cuny, T.J. Mitchison, M.A. Moskowitz, J. Yuan, Chemical inhibitor of nonapoptotic cell death with therapeutic potential for ischemic brain injury, Nat Chem Biol 1(2) (2005) 112-9.

[4] J.A. Rickard, H. Anderton, N. Etemadi, U. Nachbur, M. Darding, N. Peltzer, N. Lalaoui, K.E. Lawlor, H. Vanyai, C. Hall, A. Bankovacki, L. Gangoda, W.W. Wong, J. Corbin, C. Huang, E.S. Mocarski, J.M. Murphy, W.S. Alexander, A.K. Voss, D.L. Vaux, W.J. Kaiser, H. Walczak, J. Silke, TNFR1-dependent cell death drives inflammation in Sharpin-deficient mice, Elife 3 (2014).

[5] M. Pierdomenico, A. Negroni, L. Stronati, R. Vitali, E. Prete, J. Bertin, P.J. Gough, M. Aloi, S. Cucchiara, Necroptosis is active in children with inflammatory bowel disease and contributes to heighten intestinal inflammation, Am J Gastroenterol 109(2) (2014) 279-87.

[6] K. Newton, D.L. Dugger, A. Maltzman, J.M. Greve, M. Hedehus, B. Martin-McNulty, R.A. Carano, T.C. Cao, N. van Bruggen, L. Bernstein, W.P. Lee, X. Wu, J. DeVoss, J. Zhang, S. Jeet, I. Peng, B.S. McKenzie, M. Roose-Girma, P. Caplazi, L. Diehl, J.D. Webster, D. Vucic, RIPK3 deficiency or catalytically inactive RIPK1 provides greater benefit than MLKL deficiency in mouse models of inflammation and tissue injury, Cell Death Differ 23(9) (2016) 1565-76.

[7] T. Müller, C. Dewitz, J. Schmitz, A.S. Schröder, J.H. Bräsen, B.R. Stockwell, J.M. Murphy, U. Kunzendorf, S. Krautwald, Necroptosis and ferroptosis are alternative cell death pathways that operate in acute kidney failure, Cell Mol Life Sci 74(19) (2017) 3631-3645.

[8] J.M. Hildebrand, M. Kauppi, I.J. Majewski, Z. Liu, A.J. Cox, S. Miyake, E.J. Petrie, M.A. Silk, Z. Li, M.C. Tanzer, G. Brumatti, S.N. Young, C. Hall, S.E. Garnish, J. Corbin, M.D. Stutz, L. Di Rago, P. Gangatirkar, E.C. Josefsson, K. Rigbye, H. Anderton, J.A. Rickard, A. Tripaydonis, J. Sheridan, T.S. Scerri, V.E. Jackson, P.E. Czabotar, J.G. Zhang, L. Varghese, C.C. Allison, M. Pellegrini, G.M. Tannahill, E.C. Hatchell, T.A. Willson, D. Stockwell, C.A. de Graaf, J. Collinge, A. Hilton, N. Silke, S.K. Spall, D. Chau, V. Athanasopoulos, D. Metcalf, R.M. Laxer, A.G. Bassuk, B.W. Darbro, M.A. Fiatarone Singh, N. Vlahovich, D. Hughes, M. Kozlovskaia, D.B. Ascher, K. Warnatz, N. Venhoff, J. Thiel, C. Biben, S. Blum, J. Reveille, M.S. Hildebrand, C.G. Vinuesa, P. McCombe, M.A. Brown, B.T. Kile, C. McLean, M. Bahlo, S.L. Masters, H. Nakano, P.J. Ferguson, J.M. Murphy, W.S. Alexander, J. Silke, A missense mutation in the MLKL brace region promotes lethal neonatal inflammation and hematopoietic dysfunction, Nat Commun 11(1) (2020) 3150.

[9] S.M. Laster, J.G. Wood, L.R. Gooding, Tumor necrosis factor can induce both apoptic and necrotic forms of cell lysis, J Immunol 141(8) (1988) 2629-34.

[10] N. Holler, R. Zaru, O. Micheau, M. Thome, A. Attinger, S. Valitutti, J.L. Bodmer, P. Schneider, B. Seed, J. Tschopp, Fas triggers an alternative, caspase-8-independent cell death pathway using the kinase RIP as effector molecule, Nat Immunol 1(6) (2000) 489-95.

[11] S. He, Y. Liang, F. Shao, X. Wang, Toll-like receptors activate programmed necrosis in macrophages through a receptor-interacting kinase-3-mediated pathway, Proc Natl Acad Sci U S A 108(50) (2011) 20054-9.

[12] J. Lim, H. Park, J. Heisler, T. Maculins, M. Roose-Girma, M. Xu, B. McKenzie, M. van Lookeren Campagne, K. Newton, A. Murthy, Autophagy regulates inflammatory programmed cell death via turnover of RHIM-domain proteins, Elife 8 (2019).

[13] S.N. Schock, N.V. Chandra, Y. Sun, T. Irie, Y. Kitagawa, B. Gotoh, L. Coscoy, A. Winoto, Induction of necroptotic cell death by viral activation of the RIG-I or STING pathway, Cell Death Differ 24(4) (2017) 615-625.

[14] J. Li, T. McQuade, A.B. Siemer, J. Napetschnig, K. Moriwaki, Y.S. Hsiao, E. Damko, D. Moquin, T. Walz, A. McDermott, F.K. Chan, H. Wu, The RIP1/RIP3 necrosome forms a functional amyloid signaling complex required for programmed necrosis, Cell 150(2) (2012) 339-50.

[15] J. Zhao, S. Jitkaew, Z. Cai, S. Choksi, Q. Li, J. Luo, Z.G. Liu, Mixed lineage kinase domain-like is a key receptor interacting protein 3 downstream component of TNF-induced necrosis, Proc Natl Acad Sci U S A 109(14) (2012) 5322-7.

[16] J.M. Murphy, P.E. Czabotar, J.M. Hildebrand, I.S. Lucet, J.G. Zhang, S. Alvarez-Diaz, R. Lewis, N. Lalaoui, D. Metcalf, A.I. Webb, S.N. Young, L.N. Varghese, G.M. Tannahill, E.C. Hatchell, I.J. Majewski, T. Okamoto, R.C. Dobson, D.J. Hilton, J.J. Babon, N.A. Nicola, A. Strasser, J. Silke, W.S. Alexander, The pseudokinase MLKL mediates necroptosis via a molecular switch mechanism, Immunity 39(3) (2013) 443-53.

[17] Z. Cai, S. Jitkaew, J. Zhao, H.C. Chiang, S. Choksi, J. Liu, Y. Ward, L.G. Wu, Z.G. Liu, Plasma membrane translocation of trimerized MLKL protein is required for TNF-induced necroptosis, Nat Cell Biol 16(1) (2014) 55-65.

[18] X. Chen, W. Li, J. Ren, D. Huang, W.T. He, Y. Song, C. Yang, W. Li, X. Zheng, P. Chen, J. Han, Translocation of mixed lineage kinase domain-like protein to plasma membrane leads to necrotic cell death, Cell Res 24(1) (2014) 105-21.

[19] Y. Dondelinger, W. Declercq, S. Montessuit, R. Roelandt, A. Goncalves, I. Bruggeman, P. Hulpiau, K. Weber, C.A. Sehon, R.W. Marquis, J. Bertin, P.J. Gough, S. Savvides, J.C. Martinou, M.J. Bertrand, P. Vandenabeele, MLKL compromises plasma membrane integrity by binding to phosphatidylinositol phosphates, Cell Rep 7(4) (2014) 971-81.

[20] G. Quarato, C.S. Guy, C.R. Grace, F. Llambi, A. Nourse, D.A. Rodriguez, R. Wakefield, S. Frase, T. Moldoveanu, D.R. Green, Sequential Engagement of Distinct MLKL Phosphatidylinositol-Binding Sites Executes Necroptosis, Mol Cell 61(4) (2016) 589-601.

[21] L. Sun, H. Wang, Z. Wang, S. He, S. Chen, D. Liao, L. Wang, J. Yan, W. Liu, X. Lei, X. Wang, Mixed lineage kinase domain-like protein mediates necrosis signaling downstream of RIP3 kinase, Cell 148(1-2) (2012) 213-27.

[22] T. Xie, W. Peng, C. Yan, J. Wu, X. Gong, Y. Shi, Structural insights into RIP3-mediated necroptotic signaling, Cell Rep 5(1) (2013) 70-8.

[23] M. Huse, J. Kuriyan, The conformational plasticity of protein kinases, Cell 109(3) (2002) 275-82.

[24] S.S. Taylor, M.M. Keshwani, J.M. Steichen, A.P. Kornev, Evolution of the eukaryotic protein kinases as dynamic molecular switches, Philos Trans R Soc Lond B Biol Sci 367(1602) (2012) 2517-28.

[25] J.M. Murphy, I.S. Lucet, J.M. Hildebrand, M.C. Tanzer, S.N. Young, P. Sharma, G. Lessene, W.S. Alexander, J.J. Babon, J. Silke, P.E. Czabotar, Insights into the evolution of divergent nucleotide-binding mechanisms among pseudokinases revealed by crystal structures of human and mouse MLKL, Biochem J 457(3) (2014) 369-77.

[26] A.P. Kornev, N.M. Haste, S.S. Taylor, L.F. Eyck, Surface comparison of active and inactive protein kinases identifies a conserved activation mechanism, Proc Natl Acad Sci U S A 103(47) (2006) 17783-8.

[27] S.E. Garnish, Y. Meng, A. Koide, J.J. Sandow, E. Denbaum, A.V. Jacobsen, W. Yeung, A.L. Samson, C.R. Horne, C. Fitzgibbon, S.N. Young, P.P.C. Smith, A.I. Webb, E.J. Petrie, J.M. Hildebrand, N. Kannan, P.E. Czabotar, S. Koide, J.M. Murphy, Conformational interconversion of MLKL and disengagement from RIPK3 precede cell death by necroptosis, Nat Commun 12(1) (2021) 2211.

[28] B. Ma, D. Marcotte, M. Paramasivam, K. Michelsen, T. Wang, A. Bertolotti-Ciarlet, J.H. Jones, B. Moree, M. Butko, J. Salafsky, X. Sun, T. McKee, L.F. Silvian, ATP-Competitive MLKL Binders Have No Functional Impact on Necroptosis, PLoS One 11(11) (2016) e0165983.

[29] J.M. Hildebrand, M.C. Tanzer, I.S. Lucet, S.N. Young, S.K. Spall, P. Sharma, C. Pierotti, J.M. Garnier, R.C. Dobson, A.I. Webb, A. Tripaydonis, J.J. Babon, M.D. Mulcair, M.J. Scanlon, W.S. Alexander, A.F. Wilks, P.E. Czabotar, G. Lessene, J.M. Murphy, J. Silke, Activation of the pseudokinase MLKL unleashes the four-helix bundle domain to induce membrane localization and necroptotic cell death, Proc Natl Acad Sci U S A 111(42) (2014) 15072-7.

[30] C.L. Pierotti, M.C. Tanzer, A.V. Jacobsen, J.M. Hildebrand, J.M. Garnier, P. Sharma, I.S. Lucet, A.D. Cowan, W.J.A. Kersten, M.X. Luo, L.Y. Liang, C. Fitzgibbon, S.E. Garnish, A. Hempel, U. Nachbur, D.C.S. Huang, P.E. Czabotar, J. Silke, M.F. van Delft, J.M. Murphy, G. Lessene, Potent Inhibition of Necroptosis by Simultaneously Targeting Multiple Effectors of the Pathway, ACS Chem Biol 15(10) (2020) 2702-2713.

[31] E.J. Petrie, R.W. Birkinshaw, A. Koide, E. Denbaum, J.M. Hildebrand, S.E. Garnish, K.A. Davies, J.J. Sandow, A.L. Samson, X. Gavin, C. Fitzgibbon, S.N. Young, P.J. Hennessy, P.P.C. Smith, A.I. Webb, P.E. Czabotar, S. Koide, J.M. Murphy, Identification of MLKL membrane translocation as a checkpoint in necroptotic cell death using Monobodies, Proc Natl Acad Sci U S A 117(15) (2020) 8468-8475.

[32] A.L. Samson, Y. Zhang, N.D. Geoghegan, X.J. Gavin, K.A. Davies, M.J. Mlodzianoski, L.W. Whitehead, D. Frank, S.E. Garnish, C. Fitzgibbon, A. Hempel, S.N. Young, A.V. Jacobsen, W. Cawthorne, E.J. Petrie, M.C. Faux, K. Shield-Artin, N. Lalaoui, J.M. Hildebrand, J. Silke, K.L. Rogers, G. Lessene, E.D. Hawkins, J.M. Murphy, MLKL trafficking and accumulation at the plasma membrane control the kinetics and threshold for necroptosis, Nat Commun 11(1) (2020) 3151.

[33] H. Wang, L. Sun, L. Su, J. Rizo, L. Liu, L.F. Wang, F.S. Wang, X. Wang, Mixed lineage kinase domain-like protein MLKL causes necrotic membrane disruption upon phosphorylation by RIP3, Mol Cell 54(1) (2014) 133-146.

[34] Y. Zhang, J. Liu, D. Yu, X. Zhu, X. Liu, J. Liao, S. Li, H. Wang, The MLKL kinase-like domain dimerization is an indispensable step of mammalian MLKL activation in necroptosis signaling, Cell Death Dis 12(7) (2021) 638.

[35] Y. Meng, S.E. Garnish, K.A. Davies, K.A. Black, A.P. Leis, C.R. Horne, J.M. Hildebrand, H. Hoblos, C. Fitzgibbon, S.N. Young, T. Dite, L.F. Dagley, A. Venkat, N. Kannan, A. Koide, S. Koide, A. Glukhova, P.E. Czabotar, J.M. Murphy,

Phosphorylation-dependent pseudokinase domain dimerization drives full-length MLKL oligomerization, Nat Commun 14(1) (2023) 6804.